Cardiovasc Intervent Radiol (2019) 42:751–762
https://doi.org/10.1007/s00270-019-02175-z

LABORATORY INVESTIGATION

The Accumulation and Effects of Liposomal Doxorubicin in Tissues Treated by Radiofrequency Ablation and Irreversible Electroporation in Liver: In Vivo Experimental Study on Porcine Models

Tomáš Andrašina[1] · Josef Jaroš[2] · Tomáš Jůza[1] · Tomáš Rohan[1] · Dalibor Červinka[3] · Michal Crha[4] · Vlastimil Válek[1] · Nahum S. Goldberg[5]

Received: 30 September 2018 / Accepted: 31 January 2019 / Published online: 13 February 2019

Abstract

Purpose To compare the accumulation and effect of liposomal doxorubicin in liver tissue treated by radiofrequency ablation (RFA) and irreversible electroporation (IRE) in in vivo porcine models.

Materials and Methods Sixteen RFA and 16 IRE procedures were performed in healthy liver of two groups of three pigs. Multi-tined RFA parameters included: 100 W, target temperature 105°C for 7 min. 100 IRE pulses were delivered using two monopolar electrodes at 2250 V, 1 Hz, for 100 μsec. For each group, two pigs received 50 mg liposomal doxorubicin (0.5 mg/kg) as a drip infusion during ablation procedure, with one pig serving as control. Samples were harvested from the central and peripheral zones of the ablation at 24 and 72 h. Immunohistochemical analysis to evaluate the degree of cellular stress, DNA damage, and degree of apoptosis was performed. These and the ablation sizes were compared. Doxorubicin concentrations were also analyzed using fluorescence photometry of homogenized tissue.

Results RFA treatment zones created with concomitant administration of doxorubicin at 24 h were significantly larger than controls (2.5 ± 0.3 cm vs. 2.2 ± 0.2 cm; $p = 0.04$). By contrast, IRE treatment zones were negatively influenced by chemotherapy (2.2 ± 0.4 cm vs. 2.6 ± 0.4 cm; $p = 0.05$). At 24 h, doxorubicin concentrations in peripheral and central zones of RFA were significantly increased in comparison with untreated parenchyma (0.431 ± 0.078 μg/g and 0.314 ± 0.055 μg/g vs. 0.18 ± 0.012 μg/g; $p < 0.05$). Doxorubicin concentrations in IRE zones were not significantly different from untreated liver (0.191 ± 0.049 μg/g and 0.210 ± 0.049 μg/g vs. 0.18 ± 0.012 μg/g).

Conclusions Whereas there is an increased accumulation of periprocedural doxorubicin and an associated increase in ablation zone following RFA, a contrary effect is noted with IRE. These discrepant findings suggest that different mechanisms and synergies will need to be considered in order to select optimal adjuvants for different classes of ablation devices.

Keywords Liposomal doxorubicin · Radiofrequency ablation · Irreversible electroporation

✉ Tomáš Jůza
juza.tomas@fnbrno.cz

1 Faculty of Medicine, Department of Radiology and Nuclear Medicine, University Hospital Brno and Masaryk University, Brno, Czech Republic

2 Faculty of Medicine, Department of Histology and Embryology, Masaryk University, Brno, Czech Republic

3 Faculty of Electrical Engineering and Communication, Department of Power Electrical and Electronic Engineering, Brno University of Technology, Brno, Czech Republic

4 Faculty of Veterinary Medicine, Department of Surgery and Orthopedics, Small Animal Clinic, University of Veterinary and Pharmaceutical Sciences Brno, Brno, Czech Republic

5 Hadassah Hebrew University Medical Center, Jerusalem, Israel

Introduction

The use of local percutaneous ablation methods as a technique for the treatment of parenchymal malignancies, particularly hepatic tumors, has increased over the last 25 years [1]. Despite the differences between the principles of thermal and nonthermal methods [2], the common

objective of these techniques is to destroy malignant cells using a minimally invasive approach while sparing as much parenchyma as possible. Irrespective of the improvements in minimally invasive ablation techniques, when compared with standard of care surgical resection, the disadvantage of higher rates of local recurrence still persists for individual ablative methods [3]. In the case of thermal ablation, malignant hepatic tumors with a dimension of 2 cm and less have commensurate local recurrence rates with surgical resection, whereas for larger tumors (> 2 cm), the local recurrence rate increases [4] mainly due to inability to achieve sufficient safety margin [5].

The options for increasing the efficacy of thermal ablative methods include combining intraarterial embolization to decrease blood flow or more simply the conjunctive administration of systemic chemotherapeutic agents [6–9]. The most studied chemotherapeutic molecule in catheter-based treatment in interventional oncology is the anthracycline-containing drug doxorubicin often administered encapsulated in liposomal form. The liposomal encapsulation serves to increase safety and tolerability by decreasing cardiac and gastrointestinal toxicity, while drug is preferentially distributed to the tumor tissue, and when appropriately modified with compounds such as polyethylene glycol can increase the circulation time of the drug substantially [10]. Periprocedural administration of liposomal doxorubicin can significantly extend the volume of ablation formed by radiofrequency (RFA) [11, 12]. This combination of methods results in a high concentration of residual active metabolites within marginal zones that are susceptible to the persistence of the malignant cells that form recurrent disease [13]. In contrast to tumors treated by RFA and free doxorubicin, the intratumoral concentration of the chemotherapeutic agent after periprocedural administration of doxorubicin encapsulated in a liposomal carrier has been found to be seven times higher [14].

More recently, irreversible electroporation (IRE) has become a well-known potentially nonthermal technique for soft tissue ablation [15]. Using IRE, cell death at minimal energy input can eliminate the carbonization and heat sink effect observed in thermal methods. Additionally, the nonthermal electrical characteristic of IRE may prevent the collateral damage that can occur with thermal ablation techniques to surrounding tissues, such as the vessels, bile ducts, and nerves [16]. As true IRE is achieved only under specific electrical conditions, differences in tissue electrical conductivity can alter the homogeneity of the ablation zone, with the persistence of exclusively reversible ablated regions that have a high probability of recurrent disease. On the other hand, the marginal zones of IRE that correspond to a zone of reversible electroporation hypothetically should have the advantage of easier transportation of chemotherapeutic agents into their intracellular compartments. Indeed, this strategy has been promulgated in the past as a technique known as electrochemotherapy where the temporary formation of pores in the cellular membrane by reversible electroporation increases the efficacy of chemotherapy by facilitating the transportation of impermeable drugs of high molecular weight such as bleomycin [17]. Although free forms of anthracycline-based drugs failed to prove any laboratory benefit in combination with such reversible electroporation in prior studies [18], there has been no previous focus on liposomal forms.

Thus, we sought to assess the synergistic effect of the concomitant application of the liposomal form of doxorubicin during IRE procedures. Our study objective was to compare drug concentrations in and adjacent to the treatment zone and their effect on the size of the ablation zone compared to previously observed effects seen during the coadministration of chemotherapeutic agents to RFA treatments.

Materials and Methods

Experiments were performed under the supervision of the Veterinary Research Institute in Brno, Department of Surgery of the Faculty of Veterinary Medicine, University of Veterinary and Pharmaceutical Sciences in Brno, Czech Republic, with prior approval for the use of animal test subjects from the Ethics Committee of University of Veterinary and Pharmaceutical Sciences in Brno, Czech Republic, according to law on the protection of animals against cruelty (as amended by §17, paragraph 15 g, Act no. 246/1992 Coll.). Six laboratory female piglets (50% Duroc, 25% Pietrain, and 25% Landrace crossbreed) were split into two groups of three pigs according to the desired survival time after surgery (24 h vs. 72 h). The piglets were 4 months of age and weighed 40 ± 1 kg in the group harvested at 24 h and 32 kg ± 1 kg for those harvested after 24 h. The animals were anesthetized and given muscular blockade in a uniform fashion as described in Appendix 1. A laparotomy approach enabled direct visualization of the liver. Eight RFA and eight IRE treatments were created in the liver parenchyma of each of two groups to a maximum of three per lobe (total N of ablations = 32), (Fig. 1).

Radiofrequency energy was generated using an Angiodynamics Model 1500 generator and delivered via StarBurstXL multi-tined needles (Angiodynamics, Lantham, NY, USA) with tines extended to 3 cm. Energy parameters included: power at 100 W, target temperature of 105 °C, and procedure duration of 7 min.

IRE pulses were delivered using two monopolar electrodes using clinically relevant parameters previously

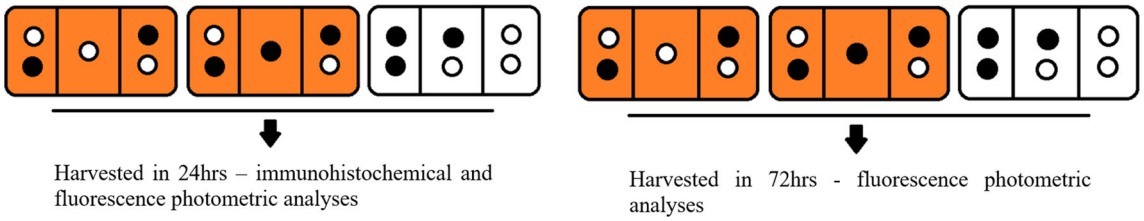

Fig. 1 Schematic representation of IRE and RF ablations for each pig. Each box represents liver parenchyma divided into three exposed lobes for thermal ablation (black filled circle) and IRE treatment (white filled circle). The orange background indicates administration of liposomal doxorubicin during treatment in slow drip infusion, while the white background indicates native control

validated in experimental studies [19–21]. These included: voltage of 2250 V, pulse length of 100 microsec, 100 pulses at a frequency of 1 Hz, a 1.5 cm electrode exposure, and electrode spacing of 1.5 ± 0.3 cm. The IRE energy was delivered by a generator prototype constructed by Department of Power Electrical and Electronic Engineering, Faculty of Electrical Engineering and Communication, Brno University of Technology, Brno, Czech Republic. Prior unpublished tests verified the accuracy of the generator output to 94% of declared values. No complications were observed either during anesthesia or any of the ablation procedures.

Long circulating liposomal doxorubicin (MYOCET 50 mg, 52.6 h half-life [10], Teva, Haarlem, NL) was intravenously administered to two of the three subjects in each group at a dose of 0.5 mg/kg at a slow drip (30 ml/60 min) while simultaneously performing the ablation. The administration was initiated 10 min prior to the first ablation procedure to achieve saturation of blood pool with liposomal doxorubicin. The third subject in each group underwent ablation without administration of the liposomal doxorubicin and hence served as a control (Fig. 1). The first group of animals was euthanized after 24 h, and the second group was euthanized after 72 h. Treatment zones were dissected from the hepatic parenchyma, and the peripheral and central zones of ablation were measured along both their long and short axes by two operators. Representative samples from each zone were immediately frozen after harvest and were stored at − 80 °C until analysis of doxorubicin content was performed. The fluorescent properties of doxorubicin were then used to quantify the amount of the drug in the obtained tissue samples as described in Appendix 2 based upon previously published procedures [14]. Additionally, representative tissue samples of each treated area including the central and peripheral zone harvested after 24 h were analyzed by the immunohistochemical protocol described in Appendix 3. Quantitative analysis was performed by measuring the thickness of the rim of staining for HSP70, γH2AX, and cleaved caspase-3 to evaluate the degree of cellular stress, DNA damage, and degree of apoptosis, respectively.

Measurements were analyzed using unpaired student's *t* tests, as appropriate, with either analytic software STATISTICA software (StatSoft CR s.r.o., Prague, Czech Republic) or Microsoft Excel (Microsoft, Redmond, Washington, USA). A *P* value of less than 0.05 was considered significant.

Results

Comparison of Treatment Zone Sizes

At 24 h, sharply demarcated borders for RFA and IRE were observed. Doxorubicin increased the overall RFA ablation size. Significant increases in gross coagulation zones were observed in the livers treated with RFA and concomitant liposomal doxorubicin administration, as compared with the liver treated with RFA alone (2.50 ± 0.30 cm vs. 2.21 ± 0.21 cm; $p = 0.04$). An increased peripheral rim of red tissue surrounding the central white region of coagulation was also observed for the RFA zones receiving doxorubicin (0.33 ± 0.05 cm vs. 0.28 ± 0.07 cm; $p = 0.04$). By contrast, after IRE treatments, ablation zones were smaller in the group administered liposomal doxorubicin (2.22 ± 0.40 cm vs. 2.63 ± 0.43 cm; $p = 0.05$). Additionally, there was poorer discrimination between central and peripheral zones for IRE (Fig. 2).

At 72 h, RF zones remained well demarcated and were slightly smaller when compared to that of 24 h (2.45 ± 0.23 cm vs. 2.11 ± 0.17 cm, respectively, $p = 0.01$). However, for IRE much more poorly defined borders were seen in 72 h to the point that an accurate representative diameter could not be assessed.

Doxorubicin Concentrations at 24 h

At 24 h, statistically significant ($p < 0.01$) differences in the concentrations of doxorubicin were seen by fluorescence photometric analysis, in both the peripheral and central zones of RF ablation. Specifically, in the peripheral and central zones of ablation, doxorubicin concentrations

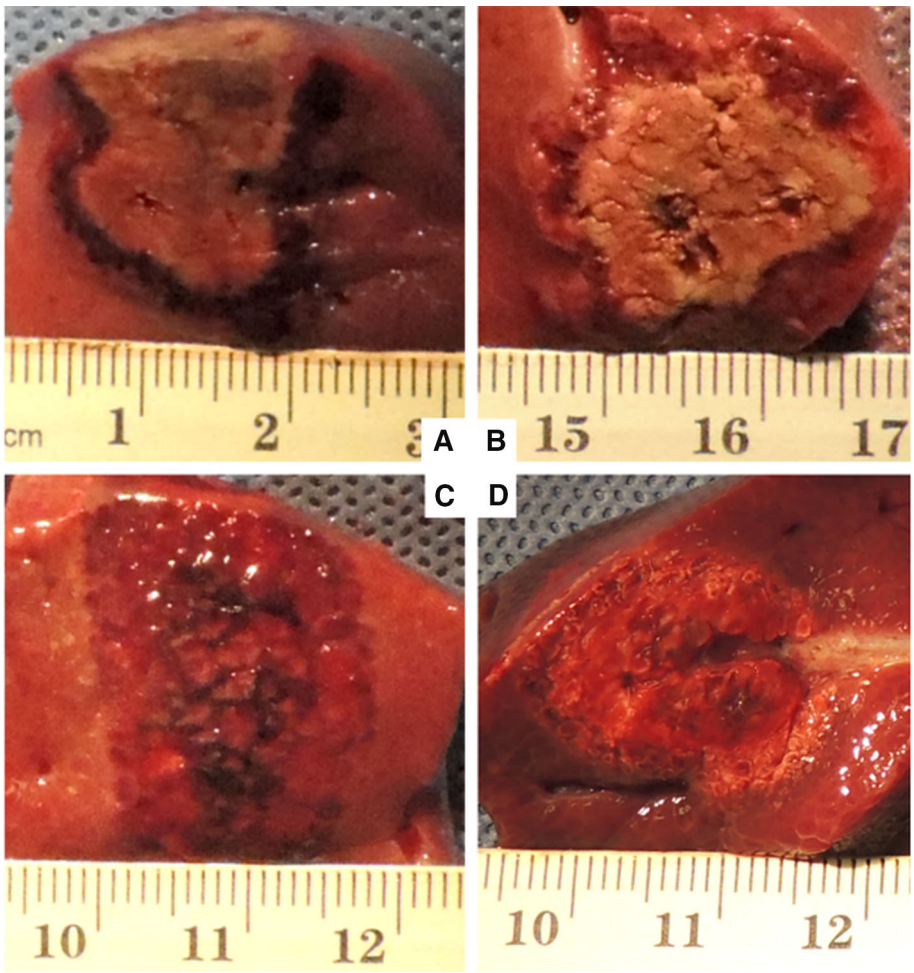

Fig. 2 Gross pathology of ablation zones. Radiofrequency ablation (**A**, **B**) and IRE treatment zones (**C**, **D**). Concomitant administration of liposomal doxorubicin (**A**, **C**), bland controls (**B**, **D**). Well-demarcated central white zone and peripheral red zone were noted for RFA, whereas a poorly defined transition is seen between central and the periphery of IRE zones

were 2.40 × and 1.74 × higher (measuring 0.431 ± 0.078 μg/g and 0.314 ± 0.055 μg/g, respectively) in comparison with the untreated parenchyma (0.180 ± 0.012 μg/g; $p < 0.01$). By contrast, low levels of doxorubicin that were equal to the untreated liver parenchyma were noted throughout the IRE treatment zones (0.191 ± 0.049 μg/g and 0.210 ± 0.049 μg/g, = 1.06; 1.17 times higher to untreated liver; $p = 0.63$, $p = 0.09$) (Fig. 3).

Doxorubicin Concentration at 72 h

At 72 h, an increased accumulation of liposomal doxorubicin was noted in RF ablation zones (0.208 ± 0.036 μg/g in central zone and 0.231 ± 0.052 μg/g in peripheral zone). These concentrations were statistically significantly higher for RFA compared to both IRE (0.18 ± 0.059 μg/g) and the non-ablated samples ($p < 0.05$, both comparisons) (Fig. 4). However, unlike at 24 h, there was no significant difference between central and peripheral RFA zones (0.208 ± 0.035 μg/g vs. 0.231 ± 0.052 μg/g, $p = 0.6$). Additionally, fluorescent intensity of doxorubicin did not show a statistically significant increase compared to unaffected parenchyma in IRE zones. For IRE, no differences between central and peripheral zones were observed.

Comparison Between Groups Harvested at 24 and 72 h

The concentration of doxorubicin in RFA zones was statistically significantly higher at 24 h than after 72 h ($p < 0.01$). There was no significant difference in these values for IRE zones $p = 0.1$ (Fig. 4). The background intensity of samples without doxorubicin administration was identical at both 24 and 72 h and corresponded to a doxorubicin concentration of 0.08 ± 0.035 μg/g.

Immunohistochemical Analyses

For RFA at 24 h, cells positively stained with HSP70 and cleaved caspase-3 were observed as a well-organized rim in the peripheral zone of ablated areas. This zone of apoptosis and cellular stress was wider with higher number of positive cells in liver treated with both RFA and

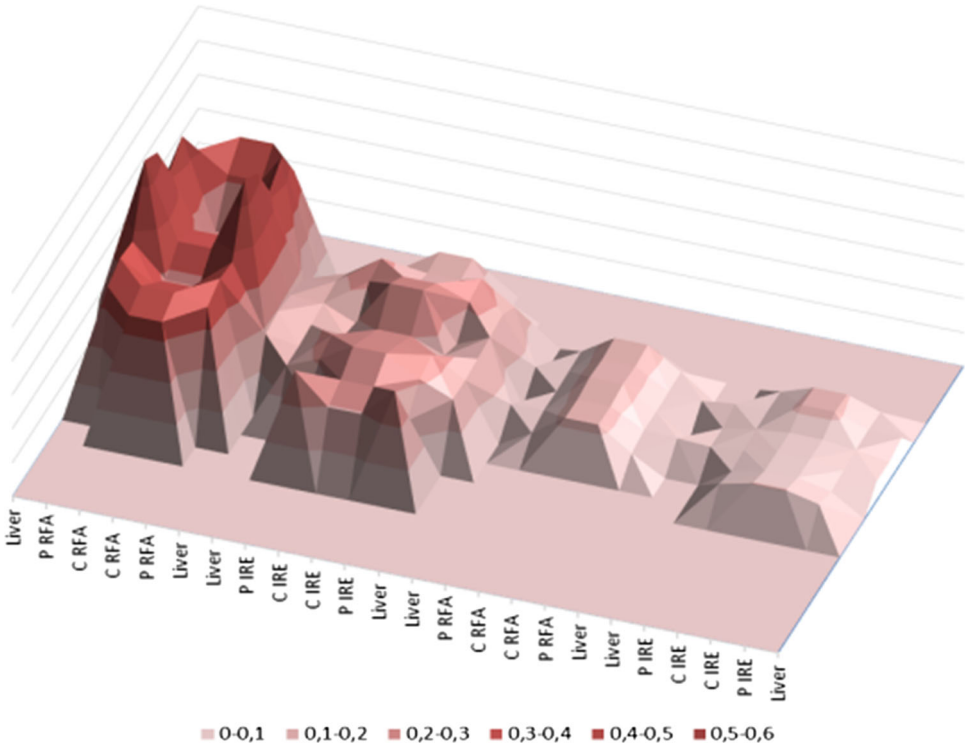

Fig. 3 Fluorescence photometric analysis of doxorubicin tissue concentration at 24 h. The surface graph depicts concentration of doxorubicin for RFA and IRE in peripheral (P) and central treatment zones (C) separated by untreated tissue (liver), two treatment zones created with concomitant administration of liposomal doxorubicin are in left part of graph

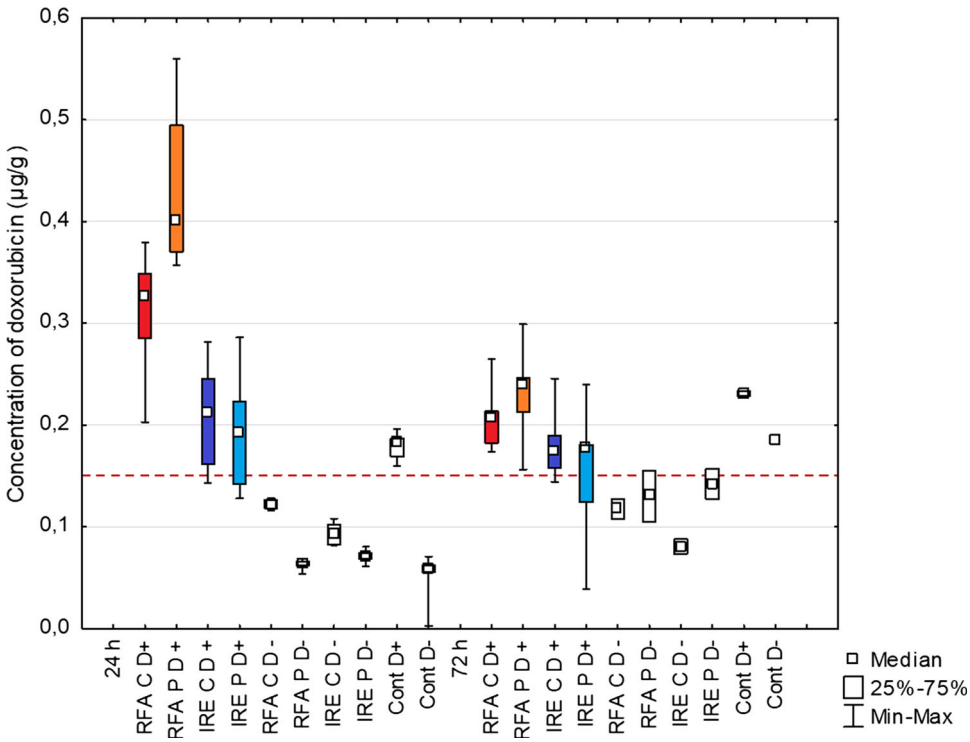

Fig. 4 Comparison of fluorescence photometric analysis results at 24 and 72 h. The red-dashed line represents background autofluorescent properties of liver tissue set to 0.15 µg/g concentration of doxorubicin (mean + 2SD)

doxorubicin than for RFA only. The rim of HSP70 positive cells was 373.6 ± 49.1 µm for combined treatment with liposomal doxorubicin compared to 222.8 ± 38.9 µm for treatment with RFA only ($p < 0.0001$); the rim of cleaved caspase-3 positive cells was 890.0 ± 162.4 µm and 587.1 ± 89.5 µm, respectively ($p < 0.0001$) (Figs. 5, 6). Cells with γH2AX positively stained nuclei created a rather narrow peripheral rim for RFA zones, which was wider for RFA alone (181.9 ± 34.2 µm) compared to that of combined therapy (133.9 ± 29.9 µm; $p < 0.0001$) (Fig. 7). No

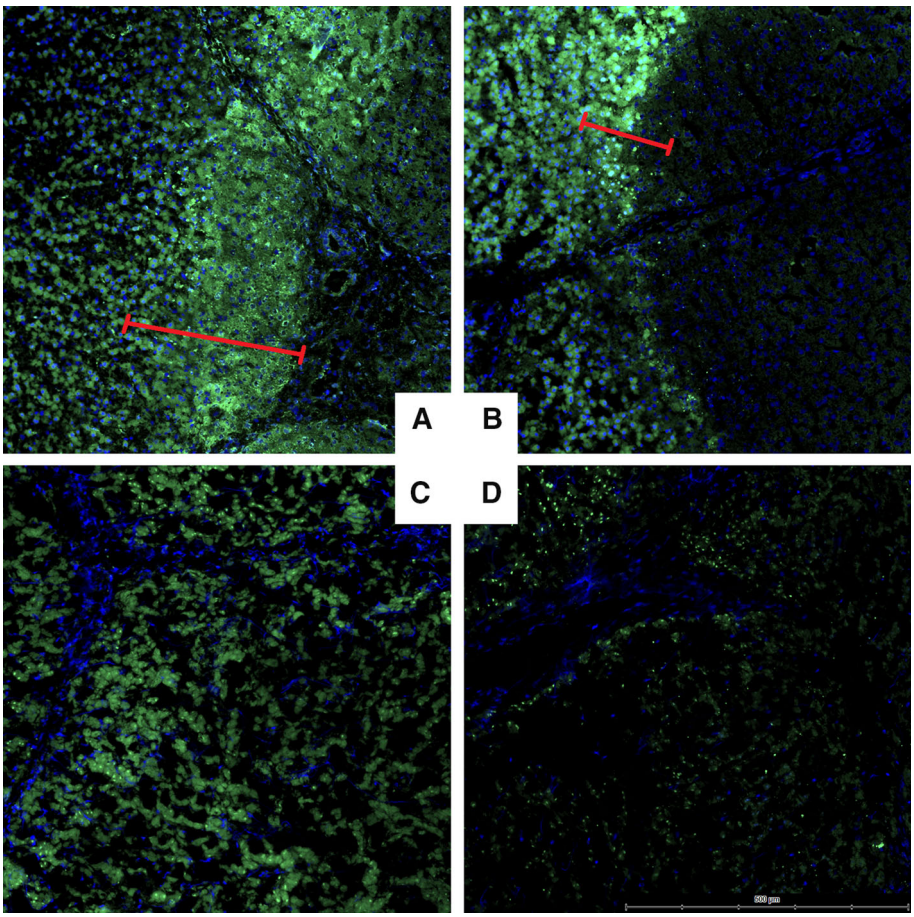

Fig. 5 Fluorescent microscopy. Peripheral zones stained with antiHSP70, RFA with liposomal doxorubicin (**A**), RFA only (**B**), IRE with liposomal doxorubicin (**C**), IRE only (**D**). Red lines showing width of positively stained borderline

measurable stained cells were seen in central zones of RFA.

For IRE zones, there were only very rarely isolated cells, without any specific distribution or dependence on doxorubicin therapy. Specifically, the central zones treated with IRE were characterized by solitary HSP positive cells, with the peripheral zones containing small groups of positive cells, most notably adjacent to interlobular septa (Fig. 5). Likewise, cleaved caspase-3 positively stained cells were predominantly located along the interlobular septa, especially in peripheral zones (Fig. 6). Moreover, no differences in expression of HSP70 and cleaved caspase-3 were noted between the group with combined therapy and IRE only. Finally, there were only very rare and isolated γH2AX positively stained cells in all tested samples (Fig. 7).

Discussion

Multiple prior studies have demonstrated that the combination of radiofrequency ablation with intravenously administered nanoparticles such as liposomal doxorubicin increases intratumoral doxorubicin accumulation and tumor destruction [14, 22]. Clinical studies with RFA show promising results as well [6]. However, there are limited data about IRE technique in combination with drug accumulation. Our work demonstrates that the treatment zones after IRE exhibit different properties than RFA zones in accumulation of doxorubicin and context with cell death. In contrast to our initial assumption, peripheral and central zones of IRE did not reach a higher accumulation of doxorubicin in comparison with unaffected healthy parenchyma. Explanations for these findings are potentially multifactorial. Prior studies have documented that accumulation of liposomal doxorubicin in tissues treated with RFA depends on many factors, e.g., drug concentration, time of administration, etc. Ahmed observed a different extent of accumulation corresponding to the temperature produced by the ablation needle, with 50 °C representing the threshold temperature for a significant difference in accumulation in tissues treated with RF compared to the control [22]. Increased temperature in tissues is responsible for endothelial injury, resulting in permeabilization of microvascularization with improved penetration of liposomal carriers [23, 24]. There is only minimal thermal effect of IRE generated by Joule heating around the electrodes during an IRE procedure. The lack of thermal injury could

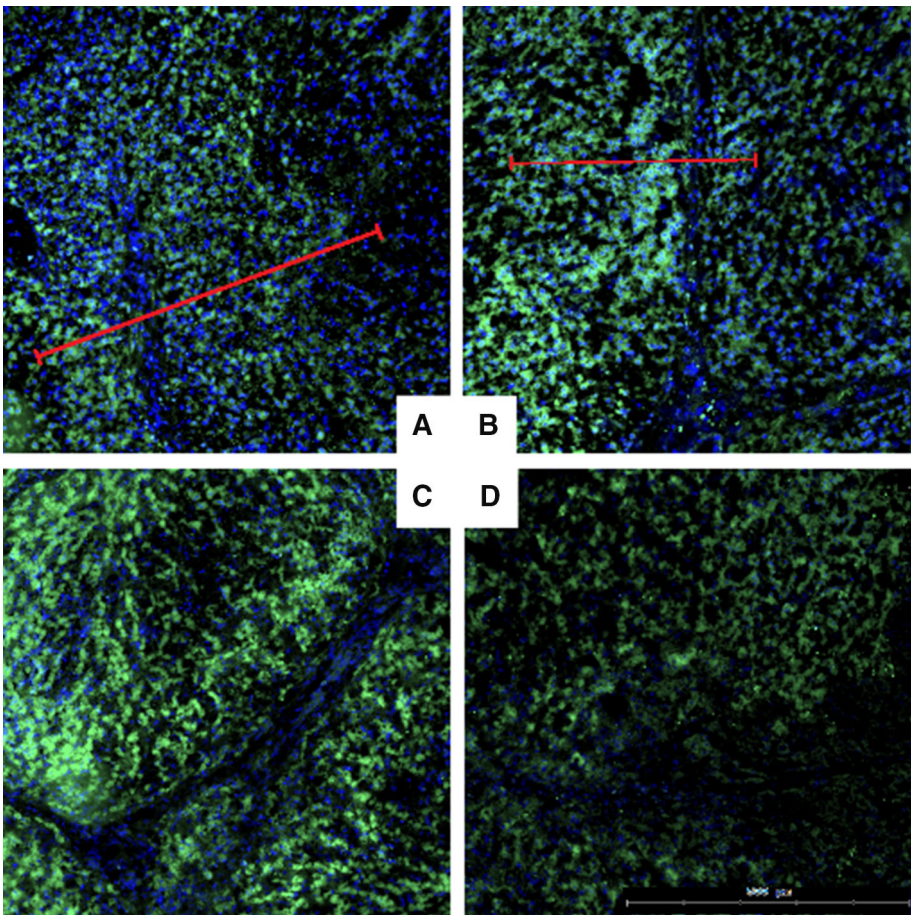

Fig. 6 Fluorescent microscopy. Peripheral zones stained with anticleaved caspase-3, RFA with liposomal doxorubicin (**A**), RFA only (**B**), IRE with liposomal doxorubicin, (**C**), IRE only (**D**). Red lines showing width of positively stained borderline

potentially partially explain why IRE, considered as a nonthermal technique, does not evince any demonstrable effect and probably brings no or minimal contribution to accumulation characteristics within the IRE zones. The very same mechanism made tumorous or inflamed tissues more susceptible to the liposomal form due to enhanced vascular permeability and retention effect (particles of 100 nm or less preferentially accumulate in diseased tissue) [11]. Macrophage infiltration of the peripheral rim with high bio-absorption of liposomal agents could be counted as another important factor as to why there is a predominant increase in accumulation within the peripheral zones of RFA. Concurrently, macrophage accumulation is higher in the border zone for RFA than for IRE ablation [25], Fig. 8 (HE staining, Appendix 3).

We simultaneously administered doxorubicin during ablative procedures. Coagulative necrosis caused by radiofrequency ablation with target temperatures reaching 100 °C leads to encapsulation of doxorubicin which circulates in the bloodstream during intervention. On the other hand, a possible persistent perfusion of the electroporated region during IRE procedure, owing to the intact vascular matrix [25], could also contribute to washout delivered drug back into the bloodstream and be another potential reason of very low accumulation of the cytostatic agent after 24 h. Moreover, RFA alone induces morphologic changes to vessels within the ablation zone lasting 12–24 h after treatment with the addition of liposomal doxorubicin causes early vessel contraction and a reduction in periablational microvascular patency [24]. So-called vascular block phenomenon which consists of a reflex constriction of arterioles and a collapse of vessels caused by hyperpermeabilization of endothelial cells could be only temporary and may not regularly occur during IRE procedures [25]. These different mechanisms could explain the fact that concentrations of doxorubicin in IRE treatment zones were identical to baseline levels of untreated parenchyma. The main aim of electrochemotherapy is local enhancement of cellular uptake in a reversibly electroporated area which would be primarily beneficial for drugs with poor natural cellular infiltration [26]. Non-permeant drugs are defined as molecules that cannot cross the plasma membrane because of hydrophilicity and absence of channels or transporters at the plasma membrane level that introduce it to intracellular compartment [27]. In comparison with bleomycin, the gold standard for electrochemotherapy, doxorubicin is hydrophobic molecule which passes naturally across biomembranes due to passive diffusion in wide

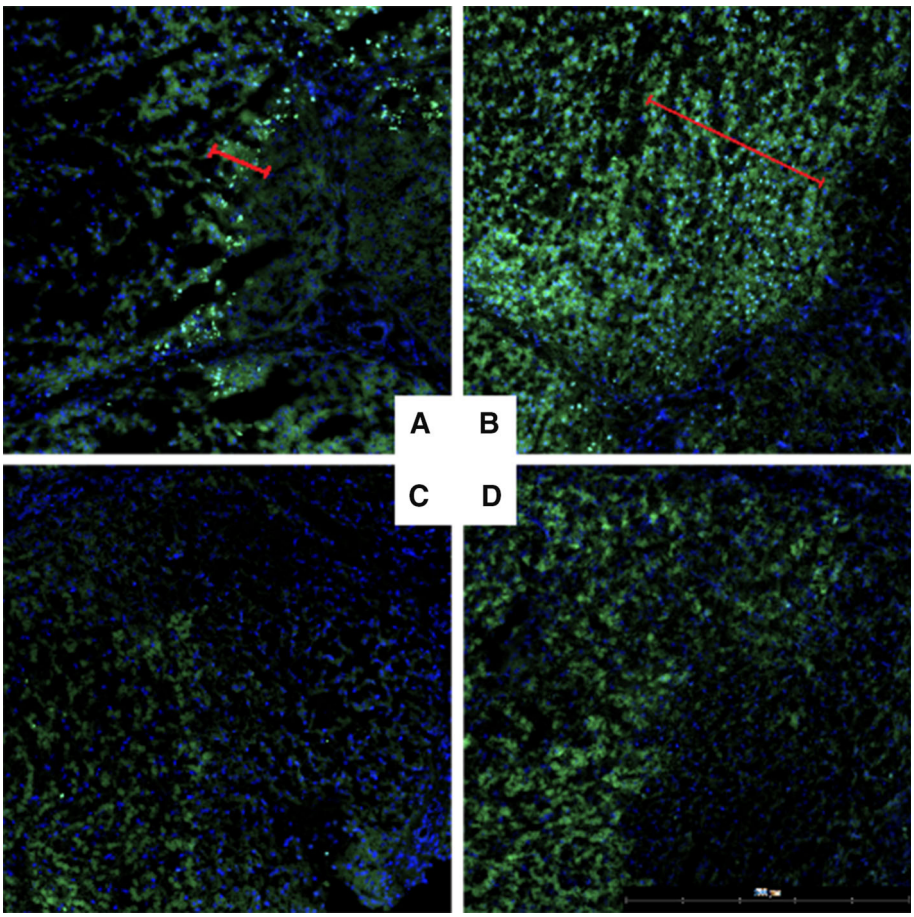

Fig. 7 Fluorescent microscopy. Peripheral zones stained with antiγH2AX, RFA with liposomal doxorubicin (**A**), RFA only (**B**), IRE with liposomal doxorubicin (**C**), IRE only (**D**). Red lines showing width of positively stained borderline

range of environments (pH, drug concentration) [28]. Thus, the development of nanocarriers for drugs such as doxorubicin has been seen as beneficial for clinical use [12, 29, 30] including when combined with RFA where increased drug accumulation was observed predominantly in post-RF inflammatory zones. Accordingly, it was initially postulated that protective liposomal nanocarriers of doxorubicin during IRE should likewise increase its utility. Yet, the poorer results of lower doxorubicin tissue concentration we obtained when combined with IRE suggest that the potential benefit of membrane permeabilization during IRE with concomitant application of liposomal doxorubicin is not always realized. Rather, unlike RFA, it is even plausible that the liposomes are directly damaged by the pulses of high voltage electric fields and lose their function and vascular leakage selectivity resulting in washout of free doxorubicin rather than tissue entrapment (Table 1).

Our observed increased size of coagulation in zones after RFA when combined with doxorubicin in vivo has been already well documented [22]. On the other hand, the shrinkage of IRE zones when combined with treatment with liposomal doxorubicin was quite surprising finding. Although the extent of hyperemia that is more robust surrounding RF zones than IRE ablation zones may potentially explain a difference in liposomal doxorubicin uptake, this finding alone does not sufficiently explain the rapid decrease in ablation size. Likewise, the limited amount of apoptosis found after IRE was unexpected particularly in light of the known increase in apoptosis after 2–6 h following IRE ablation [31, 32].

In this study, we also analyzed cell death and DNA damage, as well as heat and toxic stress in tissues by immunohistochemistry. The findings of increased bands of HSP70 and cleaved caspase-3 positive cells favoring combined treatment of RFA and liposomal forms of chemotherapy correspond to the previously cited studies [33]. Likewise, our findings for H2AX were similar for RF. However, using immunohistological staining at 24 h, we did not detect any difference in the presence of expression of HSP70 and cleaved caspase-3 between ablation zones with combined therapy and IRE treatment only. The fact HSP70 and cleaved caspase-3 predominantly identified along interlobular septa could be explained by preferential passage of electric current through areas of lower impedance (vessels etc.) [31, 34]. Likewise, no obvious borderline with γH2AX positive cells appeared in IRE zones, but only solitary and very rare γH2AX positively stained

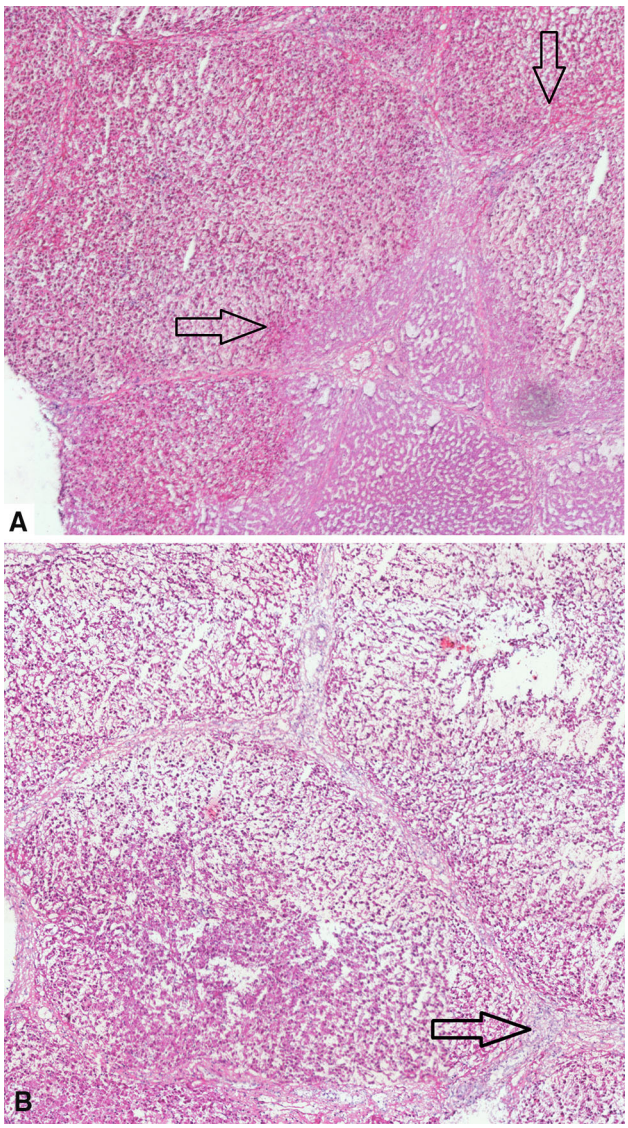

Fig. 8 H&E staining, optical magnification 200x, RFA periphery after 24 h (**A**), region of necrosis without cellular reaction, hepatocytes with eosinophilic cytoplasm and preserved nuclei sharply demarcated with hyperemic rim (arrow). IRE periphery after 24 h (**B**), H&E staining, optical magnification 200x-disintegrated hepatocytes, neutrophilic infiltrates in interlobular septs (arrow), no sharp transient zone identified

cells in all tested samples may be elucidated by the long-time period after treatment.

To account for the IRE findings, we note that apoptosis is a relatively intensive and rapid process with broad spectrum of morphological cellular changes. Maximal caspase activation is achieved very shortly in 1–4 h, and at that time many of the characteristic features of apoptosis that are relevant to cell clearance are visible [35]. The work of Al-Sakere also shows that most of DNA breaks appear only few hours after treatment with no organized cell nuclei after 24 h [36]. Indeed, it has been noted that in as little as a few hours following IRE that the cellular diameter is reduced (25–50%) and by 12–24 h, the cellular diameter is again increased by 10–30%. Thus, based upon the known more rapid apoptosis and cell death when combining liposomal doxorubicin with RFA, we postulate that more rapid apoptosis may have occurred with IRE and due to persistent vascularity and increased scavenger cells, there was quicker clearance of the treatment zone [25]. Indeed, Solazzo et al. observed a more rapid H2AX peak and clearance for RFA and liposomal doxorubicin (1 and 4 h respectively, compared to RFA alone (peak at 4 h) [33]. Thus, any chemotherapeutical influence upon the apoptotic process may be difficult to evaluate from one-time interval, and without further detailed kinetic studies, it may be very challenging to assess the precise treatment zone. Future work which includes earlier follow-up may shed more light on this issue. Regardless, if this hypothesis is correct, it will draw more attention to problems of accurate measurement of ablation extent, when there is rapid clearing due to apoptosis or other currently unidentified other mechanism or response of the body. Most notably, in our case, increased and accelerated damage to cellular constituents which leads to apoptosis could be the key factor explaining smaller size of measured ablative zones in 24 h after ablation.

The peaking concentrations of chemotherapeutic we observed at 24 h after RFA treatment is in agreement with some previous publications [14]. However, others using a different liposome preparation have reported 72-h interval as

Table 1 Sizes of RFA and IRE zones. Significant differences in maximal zone diameter are marked with bold (D+ with administration of liposomal doxorubicin, D− without administration of liposomal agent)

Size in cm (average)	Total		Centre		Periphery	
	Min	Max	Min	Max	Min	Max
RFA D+	1.74 ± 0.19	**2.50 ± 0.30**	1.31 ± 0.19	2.01 ± 0.23	0.12 ± 0.03	**0.33 ± 0.05**
RFA D−	1.71 ± 0.33	**2.21 ± 0.21**	1.21 ± 0.34	1.77 ± 0.30	0.12 ± 0.03	**0.28 ± 0.07**
IRE D+	1.54 ± 0.28	**2.22 ± 0.40**	**0.95 ± 0.27**	**1.59 ± 0.37**	0.20 ± 0.11	0.39 ± 0.17
IRE D−	1.68 ± 0.33	**2.63 ± 0.42**	**1.29 ± 0.18**	**2.10 ± 0.51**	0.13 ± 0.04	0.28 ± 0.08

more efficient [37, 38]. This suggests that tailoring of drug administration will be needed for each nanopreparation and for each ablation energy source. Regardless, the combination of IRE with the liposomal doxorubicin preparation selected will likely be less ideal for clinical usage than its combination with RFA. Indeed, from the clinical perspective, our results suggest that combining the liposomal form of doxorubicin with RFA should not likely be replaced by combining liposomal carriers with IRE until there is demonstration of either improved or equivalent efficacy, and ideally a better mechanism of action will be demonstrated.

There are several limitations of our study. The experiments were performed on a single tissue model only (i.e., normal porcine liver), and the ablation methods were not employed within cancer tissues or other types of baseline lives (e.g steatosis and fibrosis). On the basis of previous studies, doxorubicin accumulation within tumorous tissues seems to be clearly influenced by RF ablation with substantial increases in concentration being observed at the periphery of the RF treatment zone in cancerous tissues. Commonly, cancer cells show higher sensitivity to doxorubicin and usually faster DNA metabolism of cancer cells could trigger more cells to apoptotic pathways compared to healthy parenchyma [39, 40]. Regardless, we acknowledge that our experiments performed on liver parenchyma provide us only first predictions of principles which could be used in concomitant treatment of liposomal chemotherapy and IRE. Clearly, the treatment of other tissue types—most notably cancers—will be needed to draw more definitive conclusions. Likewise, additional study with a more varied set of IRE and drug parameters could potentially enhance our understanding of this increased resorption phenomenon.

Conclusion

Our study has verified enhanced uptake of liposomal doxorubicin within RFA treatment zones as previously described with fluorescence photometric analyses showing maximal concentrations of doxorubicin in the peripheral zone of RFA after 24 h. On the contrary, IRE zones do not achieve a significant accumulation of liposomal doxorubicin compared to unaffected parenchyma. Thus, our initial hypothesis of a synergistic effect of combined administration of liposomal doxorubicin and IRE treatment was not proven. In contrast, a decreased size of IRE treatment zones with concomitant administration of liposomal doxorubicin was observed, a completely opposite finding in comparison with enhancing effect of these liposomes in combination with RFA procedure. Thus, our work calls for further clinical work optimizing ideal combinations of specific ablation tools and drug formulations and for more basic research elucidating the underlying mechanisms of action to achieve optimal therapeutic results.

Acknowledgments This study was supported by Ministry of Health of the Czech Republic, Grant No. 15-32484a, and supported by funds from the Faculty of Medicine MU to junior researcher Tomáš Andrašina.

Compliance with Ethical Standards

Conflict of interest Author Nahum S. Goldberg is a consultant to Angiodynamics, Inc. and Cosman Medical Inc.

Ethical Approval All applicable international, national, and institutional guidelines for the care and use of animals were followed. All procedures performed in studies involving animals were in accordance with the ethical standards of the institution or practice at which the studies were conducted.

Informed Consent For this type of study, informed consent is not required.

Consent for Publication For this type of study, consent for publication is not required.

Appendix 1: Supplementary Animal Information

The pigs were housed in stone hutches under controlled environmental conditions (20–22 °C room temperature, 50–60% relative humidity, 12 h light and 12 h dark cycle). The whole procedure was carried out under general anesthesia with deep muscle relaxation, and the animals were intubated and artificially ventilated. The following combinations of substances were applied for general anesthesia. Premedication: i.m. Tiletamine 2 mg/kg + zolazepam 2 mg/kg (Zoletil 100, Virbac) + ketamine 2 mg/kg (Narketan, Vetoquinol) + xylazine 2 mg/kg (Sedazine, Fort Dodge) i.v. cannulation + Buprenorphine (Temgesic, Schering-Plow) 0.01 mg/kg i.m. Induction: Norofol (propofol, Fresenius) to effect (1–2 mg/kg) i.v. Lateral ear vein was used for catheterization. Conduction: Inhalation anesthesia of O2–air mixtures- Isoflurane (Aerrane, Baxter) Monitoring: HR, RR, SpO2, ETCO2. Atracrium (1.5 mg/kg, Tracurium, GlaxoSmithKline, Italy) was used for muscle relaxation. Each animal underwent median laparotomy whereby the dominant surface of liver was exposed. After surgery, the animals were awakened and pain was efficiently controlled by meloxicam (0.2 mg/kg, Metacam 5 mg/mL, Boehringer Ingelheim, Germany). The animals were euthanized 24 and 72 h after surgery (Thiopental, T61 *Intervet International* GmbH). In each pig, an en bloc specimen of liver was excised.

Appendix 2: Supplementary Laboratory Information

Briefly, specified tissues were harvested, weighed, and homogenized with a MagNA Lyser (Roche, Basel, CH) in acid alcohol (0.3 *N* hydrochloric acid, 70% ethyl alcohol). Doxorubicin was extracted for 24 h at 5 °C. The extracted

doxorubicin supernatant from all tissue homogenate samples was quantified with fluorescence photometry using an excitation wavelength of 485 nm while measuring the intensity of the emission at 535–595 nm. The obtained concentrations were plotted on a standard curve of liposomal doxorubicin serially diluted likewise in acid alcohol. Considering fluorescence photometry analysis, we note that the absolute values of concentration of doxorubicin in liver tissue homogenate were influenced by autofluorescent properties of physiologically presented molecules such as cytochromes in liver tissue. Nevertheless, these natural backgrounds could be statistically distinguished from tissue treated with liposomal doxorubicin.

Appendix 3: Supplementary Laboratory Information

Representative tissue samples of each treated area from central and peripheral zone harvested after 24 h were embedded in OCT compound (Leica), snap-frozen, and stored at −20 °C. The "central zone" was defined as the 1 cm most central part of the treated area, and the "peripheral zone" was defined as the tissue 2–3 mm nearest to "apparently normal surrounding liver parenchyma." Tissues were sectioned on a Leica Cryostat (7 μm) and placed on treated slides for fluorescent analysis. Sections were counterstained with 4′, 6-diamidino-2-phenylindole (DAPI) (Sigma-Aldrich) and mounted with 80% glycerol mounting medium for fluorescent microscopic analysis using TissueFax (TissueGnostics). A two-step immunohistochemical protocol was performed: primary antibodies for specific antigens included HSP70 (Assay Designs, Ann Arbor, Mich) to assess for cellular stress; γH2AX (Cell Signaling Technologies, Danvers, Mass) as a marker of DNA damage; and cleaved caspase-3 (Cell Signaling Technologies) as a marker of apoptosis and secondary staining with fluorochrome. Images of whole sections were automatically acquired with 10*x*/0.45 objective for two channels (405/450 nm excitation/emission, 488/535 nm ex/em). Quantitative analysis was performed by measuring thickness of the rim of staining, from each central and peripheral ablation zone, and four random fields were analyzed.

References

1. Yu H, Burke CT. Comparison of percutaneous ablation technologies in the treatment of malignant liver tumors. Semin Interv Radiol. 2014;31:129–37. https://doi.org/10.1055/s-0034-1373788.
2. Ahmed M, Brace CL, Lee FT, Goldberg SN. Principles of and advances in percutaneous ablation. Radiology. 2011;258:351–69. https://doi.org/10.1148/radiol.10081634.
3. van Amerongen MJ, Jenniskens SFM, van den Boezem PB, Fütterer JJ, de Wilt JHW. Radiofrequency ablation compared to surgical resection for curative treatment of patients with colorectal liver metastases—a meta-analysis. HPB. 2017;19:749–56. https://doi.org/10.1016/j.hpb.2017.05.011.
4. Lei JY, Wang WT, Yan LN, Wen TF, Li B. Radiofrequency ablation versus surgical resection for small unifocal hepatocellular carcinomas. Medicine (Baltimore). 2014. https://doi.org/10.1097/md.0000000000000271.
5. Wang X, Sofocleous CT, Erinjeri JP, Petre EN, Gonen M, Do KG, Brown KT, Covey AM, Brody LA, Alago W, Thornton RH, Kemeny NE, Solomon SB. Margin size is an independent predictor of local tumor progression after ablation of colon cancer liver metastases. Cardiovasc Intervent Radiol. 2013;36:166–75. https://doi.org/10.1007/s00270-012-0377-1.
6. Goldberg SN, Kamel IR, Kruskal JB, Reynolds K, Monsky WL, Stuart KE, Ahmed M, Raptopoulos V. Radiofrequency ablation of hepatic tumors: increased tumor destruction with adjuvant liposomal doxorubicin therapy. Am J Roentgenol. 2002;179:93–101. https://doi.org/10.2214/ajr.179.1.1790093.
7. Tang C, Shen J, Feng W, Bao Y, Dong X, Dai Y, Zheng Y, Zhang J. Combination therapy of radiofrequency ablation and transarterial chemoembolization for unresectable hepatocellular carcinoma: a retrospective study. Medicine (Baltimore). 2016;95:e3754. https://doi.org/10.1097/MD.0000000000003754.
8. Tanaka T, Isfort P, Braunschweig T, Westphal S, Woitok A, Penzkofer T, Bruners P, Kichikawa K, Schmitz-Rode T, Mahnken AH. Superselective particle embolization enhances efficacy of radiofrequency ablation: effects of particle size and sequence of action. Cardiovasc Intervent Radiol. 2013;36:773–82. https://doi.org/10.1007/s00270-012-0497-7.
9. Yamakado K, Inaba Y, Sato Y, Yasumoto T, Hayashi S, Yamanaka T, Nobata K, Takaki H, Nakatsuka A. Radiofrequency ablation combined with hepatic arterial chemoembolization using degradable starch microsphere mixed with mitomycin c for the treatment of liver metastasis from colorectal cancer: a prospective multicenter study. Cardiovasc Intervent Radiol. 2017;40:560–7. https://doi.org/10.1007/s00270-016-1547-3.
10. Mross K, Niemann B, Massing U, Drevs J, Unger C, Bhamra R, Swenson CE. Pharmacokinetics of liposomal doxorubicin (TLC-D99; Myocet) in patients with solid tumors: an open-label, single-dose study. Cancer Chemother Pharmacol. 2004;54:514–24. https://doi.org/10.1007/s00280-004-0825-y.
11. Andriyanov AV, Koren E, Barenholz Y, Goldberg SN. Therapeutic efficacy of combining pegylated liposomal doxorubicin and radiofrequency (rf) ablation: comparison between slow-drug-releasing, non-thermosensitive and fast-drug-releasing thermosensitive nano-liposomes. PLoS ONE. 2014. https://doi.org/10.1371/journal.pone.0092555.
12. Goldberg SN, Girnan GD, Lukyanov AN, Ahmed M, Monsky WL, Gazelle GS, Huertas JC, Stuart KE, Jacobs T, Torchillin VP, Halpern EF, Kruskal JB. Percutaneous tumor ablation: increased necrosis with combined radio-frequency ablation and intravenous liposomal doxorubicin in a rat breast tumor model. Radiology. 2002;222:797–804. https://doi.org/10.1148/radiol.2223010861.
13. Ahmed M, Moussa M, Goldberg SN. Synergy in cancer treatment between liposomal chemotherapeutics and thermal ablation. Chem Phys Lipids. 2012;165:424–37. https://doi.org/10.1016/j.chemphyslip.2011.12.002.
14. Monsky WL, Kruskal JB, Lukyanov AN, Girnun GD, Ahmed M, Gazelle GS, Huertas JC, Stuart KE, Torchilin VP, Goldberg SN. Radio-frequency ablation increases intratumoral liposomal doxorubicin accumulation in a rat breast tumor model. Radiology. 2002;224:823–9. https://doi.org/10.1148/radiol.2243011421.
15. Lyu T, Wang X, Su Z, Shangguan J, Sun C, Figini M, Wang J, Yaghmai V, Larson AC, Zhang Z. Irreversible electroporation in

primary and metastatic hepatic malignancies. Medicine (Baltimore). 2017. https://doi.org/10.1097/md.0000000000006386.
16. Deipolyi AR, Golberg A, Yarmush ML, Arellano RS, Oklu R. Irreversible electroporation: evolution of a laboratory technique in interventional oncology. Diagn Interv Radiol. 2014;20:147–54. https://doi.org/10.5152/dir.2013.13304.
17. Miklavčič D, Serša G, Brecelj E, Gehl J, Soden D, Bianchi G, Ruggieri P, Rossi CR, Campana LG, Jarm T. Electrochemotherapy: technological advancements for efficient electroporation-based treatment of internal tumors. Med Biol Eng Comput. 2012;50:1213–25. https://doi.org/10.1007/s11517-012-0991-8.
18. Gehl J, Skovsgaard T, Mir LM. Enhancement of cytotoxicity by electropermeabilization: an improved method for screening drugs. Anticancer Drugs. 1998;9:319–25.
19. Ben-David E, Appelbaum L, Sosna J, Nissenbaum I, Goldberg SN. Characterization of irreversible electroporation ablation in in vivo porcine liver. Am J Roentgenol. 2012;198:W62–8. https://doi.org/10.2214/AJR.11.6940.
20. Appelbaum L, Ben-David E, Faroja M, Nissenbaum Y, Sosna J, Goldberg SN. Irreversible electroporation ablation: creation of large-volume ablation zones in in vivo porcine liver with four-electrode arrays. Radiology. 2013;270:416–24. https://doi.org/10.1148/radiol.13130349.
21. Rubinsky B, Onik G, Mikus P. Irreversible electroporation: a new ablation modality–clinical implications. Technol Cancer Res Treat. 2007;6:37–48. https://doi.org/10.1177/153303460700600106.
22. Ahmed M, Liu Z, Lukyanov AN, Signoretti S, Horkan C, Monsky WL, Torchilin VP, Goldberg SN. Combination radiofrequency ablation with intratumoral liposomal doxorubicin: effect on drug accumulation and coagulation in multiple tissues and tumor types in animals. Radiology. 2005;235:469–77. https://doi.org/10.1148/radiol.2352031856.
23. Kruskal JB, Oliver B, Huertas JC, Goldberg SN. Dynamic intrahepatic flow and cellular alterations during radiofrequency ablation of liver tissue in mice. J Vasc Interv Radiol JVIR. 2001;12:1193–201.
24. Moussa M, Goldberg SN, Tasawwar B, Sawant RR, Levchenko T, Kumar G, Torchilin VP, Ahmed M. Adjuvant liposomal doxorubicin markedly affects radiofrequency (RF) ablation-induced effects on periablational microvasculature. J Vasc Interv Radiol JVIR. 2013;24:1021–33. https://doi.org/10.1016/j.jvir.2013.03.006.
25. Bulvik BE, Rozenblum N, Gourevich S, Ahmed M, Andriyanov AV, Galun E, Goldberg SN. Irreversible electroporation versus radiofrequency ablation: a comparison of local and systemic effects in a small-animal model. Radiology. 2016;280:413–24. https://doi.org/10.1148/radiol.2015151166.
26. Neal RE, Rossmeisl JH, D'Alfonso V, Robertson JL, Garcia PA, Elankumaran S, Davalos RV. In Vitro and numerical support for combinatorial irreversible electroporation and electrochemotherapy glioma treatment. Ann Biomed Eng. 2014;42:475–87. https://doi.org/10.1007/s10439-013-0923-2.
27. Mir LM, Orlowski S. Mechanisms of electrochemotherapy. Adv Drug Deliv Rev. 1999;35:107–18. https://doi.org/10.1016/S0169-409X(98)00066-0.
28. Speelmans G, Staffhorst RWHM, Steenbergen HG, de Kruijff B. Transport of the anti-cancer drug doxorubicin across cytoplasmic membranes and membranes composed of phospholipids derived from *Escherichia coli* occurs via a similar mechanism. Biochim Biophys Acta BBA Biomembr. 1996;1284:240–6. https://doi.org/10.1016/S0005-2736(96)00137-X.
29. O'Shaughnessy JA. Pegylated liposomal doxorubicin in the treatment of breast cancer. Clin Breast Cancer. 2003;4:318–28.
30. Rafiyath SM, Rasul M, Lee B, Wei G, Lamba G, Liu D. Comparison of safety and toxicity of liposomal doxorubicin vs. conventional anthracyclines: a meta-analysis. Exp Hematol Oncol. 2012;1:10. https://doi.org/10.1186/2162-3619-1-10.
31. Faroja M, Ahmed M, Appelbaum L, Ben-David E, Moussa M, Sosna J, Nissenbaum I, Goldberg SN. Irreversible electroporation ablation: Is all the damage nonthermal? Radiology. 2013;266:462–70. https://doi.org/10.1148/radiol.12120609.
32. Guo Y, Zhang Y, Klein R, Nijm GM, Sahakian AV, Omary RA, Yang G-Y, Larson AC. Irreversible electroporation therapy in the liver: longitudinal efficacy studies in a rat model of hepatocellular carcinoma. Cancer Res. 2010;70:1555–63. https://doi.org/10.1158/0008-5472.CAN-09-3067.
33. Solazzo SA, Ahmed M, Schor-Bardach R, Yang W, Girnun GD, Rahmanuddin S, Levchenko T, Signoretti S, Spitz DR, Torchilin V, Goldberg SN. Liposomal doxorubicin increases radiofrequency ablation–induced tumor destruction by increasing cellular oxidative and nitrative stress and accelerating apoptotic pathways1. Radiology. 2010;255:62–74. https://doi.org/10.1148/radiol.09091196.
34. Ruarus AH, Vroomen LGPH, Puijk RS, Scheffer HJ, Faes TJC, Meijerink MR. Conductivity rise during irreversible electroporation: True permeabilization or heat? Cardiovasc Intervent Radiol. 2018;41:1257–66. https://doi.org/10.1007/s00270-018-1971-7.
35. Elliott MR, Ravichandran KS. The dynamics of apoptotic cell clearance. Dev Cell. 2016;38:147–60. https://doi.org/10.1016/j.devcel.2016.06.029.
36. Al-Sakere B, André F, Bernat C, Connault E, Opolon P, Davalos RV, Rubinsky B, Mir LM. Tumor ablation with irreversible electroporation. PLoS ONE. 2007. https://doi.org/10.1371/journal.pone.0001135.
37. Ahmed M, Monsky WE, Girnun G, Lukyanov A, D'Ippolito G, Kruskal JB, Stuart KE, Torchilin VP, Goldberg SN. Radiofrequency thermal ablation sharply increases intratumoral liposomal doxorubicin accumulation and tumor coagulation. Cancer Res. 2003;63:6327–33.
38. Moussa M, Goldberg SN, Kumar G, Sawant RR, Levchenko T, Torchilin VP, Ahmed M. Nanodrug-enhanced radiofrequency tumor ablation: effect of micellar or liposomal carrier on drug delivery and treatment efficacy. PLoS ONE. 2014;9:e102727. https://doi.org/10.1371/journal.pone.0102727.
39. Cox J, Weinman S. Mechanisms of doxorubicin resistance in hepatocellular carcinoma. Hepatic Oncol. 2016;3:57–9. https://doi.org/10.2217/hep.15.41.
40. Thorn CF, Oshiro C, Marsh S, Hernandez-Boussard T, McLeod H, Klein TE, Altman RB. Doxorubicin pathways: pharmacodynamics and adverse effects. Pharmacogenet Genomics. 2011;21:440–6. https://doi.org/10.1097/FPC.0b013e32833ffb56.